

ELECTRONIC SUPPLEMENTARY INFORMATION

Inherent heterogeneities and nanostructural anomalies in organic glasses revealed by EPR

Mikhail Yu. Ivanov,^{†,*} Olga D. Bakulina,^{†,‡} Dmitriy V. Alimov,[‡] Sergey A. Prikhod'ko,[§]
Sergey L. Veber,[†] Svetlana Pylaeva,^{||} Nicolay Yu. Adonin,[§] Matvey V. Fedin^{†,*}

[†] *International Tomography Center SB RAS, Institutskaya Street 3a, 630090 Novosibirsk, Russia*

[‡] *Novosibirsk State University, Pirogova Street 2, 630090 Novosibirsk, Russia*

[§] *Boriskov Institute of Catalysis SB RAS, Lavrentiev Avenue 5, 630090 Novosibirsk, Russia*

^{||} *Universität Paderborn, Warburger Str. 100, 33098 Paderborn, Germany*

Table of Contents

I Experimental section	2
II Differential scanning calorimetry (DSC) measurements.....	3
III Molecular dynamics: supplementary details.....	7
IV EPR of stochastic molecular librations	8
V Temperature dependence of T_2 relaxation time	11
VI Continuous wave EPR spectra.....	13
References.....	16

I Experimental section

Dimethyl phthalate (DMP), diethyl phthalate (DEP), di-n-butyl phthalate (DBP), and di-n-octyl phthalate (DOP) were purchased from Hromresurs, ethanol from Kemerovo Pharmaceutical Factory, 1-butanol from Chemical Line, 1-pentanol from Ural base of chemical reagents, 1-hexanol from Vecton. Ethylbenzene was purchased from Acros and purified by distillation. Buthylbenzene was synthesized according to the procedures described in Ref.S1

The spiro-cyclohexane-substituted nitroxide N1 (14-carbamoyl-7-azadispiro[5.1.5.2]pentadeca-14-ene-7-oxyl) was prepared according to literature protocol.^{S2}

2,2,6,6-Tetramethylpiperidine-1-oxyl-D₁₈ (TEMPO-D₁₈) was prepared from TAA-D₁₇ in analogy to literature procedure for non-deuterated compound.^{S3} The perdeutero-2,2,5,5-tetramethylpiperidin-4-one (TAA-D₁₇) was prepared from NH₄Cl and acetone-D₆ in analogy to the procedure described in Ref.S4. To remove the trace of carbon tetrachloride the crystallosolvate was dissolved in the mixture THF-diethyl ether and evaporated in vacuum, the residue was dissolved in hexane and evaporated again.

Deuterium oxide D₂O (5 ml, 0.25 mol) was added to a mixture of triethylene glycol (10.6 mL, 0.078 mol) and KOH (2.42 g, 0.043 mol) upon stirring and then water was distilled off (heating up to 150 °C) and the mixture was allowed to cool down to ambient temperature. The procedure was repeated 5 times to provide enrichment with deuterium. Then a new portion of D₂O (2 ml, 0.1 mol) and hydrazine-D₄ (2 ml, 0.055 mol) were added and the mixture was stirred until homogeneous solution formed, TAA-D₁₇ (3.44 g, 0.02 mol) was added and the mixture was stirred under reflux (135-145 °C) for 1 h. Then the reaction mixture was allowed to cool to ambient temperature, the reflux condenser was replaced with adapter with Liebig condenser and the reaction mixture was gradually heated to 195 °C, collecting distillate. The mixture was saturated with K₂CO₃, the organic layer was separated, dried with K₂CO₃ and distilled, collecting the fraction with b.p. 145-160 °C. The crude HTMP-D₁₉ was poured into the solution of Na₂WO₄ dihydrate (0.33 g, 1 mmol) and EDTA disodium salt (0.186 g, 0.5 mmol) in 50% aqueous methanol (10 ml), cooled down to 10 °C and hydrogen peroxide 30% was added by portions 0.15 ml each 12 h. The reaction mixture was allowed to stand for two weeks, then saturated with K₂CO₃ and extracted with pentane. The extract was washed with 5% NaHSO₄, and dried with CaCl₂. The pentane was distilled off at atmospheric pressure, the residue was diluted with pentane (10% volume) and cooled to -18 °C for crystallization. The dark-red crystals of TEMPO-D₁₈ were filtered off and washed with small amount of very cold pentane (-150 °C), yield 0.83 g (24%), m.p. 36-38 °C; Mass spectrum, M+, (%): 175 (11), 174 (100), 173 (67), 172 (31), 171 (14), 170 (7), 169 (3); isotope enrichment roughly estimated from the mass spectrum >95%.

The final concentration of spin probe in a sample was about 1 mM.

In the case of phthalates samples nitroxides were dissolved in the corresponding phthalate in concentrations of ~1 mM. Next, for N1 containing samples, the solution was placed in the EPR quartz tube (inner diameter of 2.8 mm), evacuated at 10^{-5} mbar (samples with spiro-cyclohexane-substituted nitroxide radical were simultaneously heated at 85 °C) for 12 hours to reduce the amount of remaining water and to eliminate the remaining oxygen, exposed to 3–5 freeze–pump–thaw cycles, and finally sealed off under vacuum. Samples with TEMPO-D₁₈ were prepared in the same way but without heating during pumping to avoid radical reduction.

Preparation of samples of alcohols and substituted benzenes differs in the pumping method. The solution was also placed in the EPR quartz tube, and because of its high volatility it was exposed to 3–5 freeze–pump–thaw cycles and sealed off under vacuum while the sample was placed in liquid nitrogen.

Pulse EPR measurements were performed using a commercial Bruker Elexsys E580 spectrometer at X-band. The spectrometer was equipped with an Oxford Instruments temperature control system (4–300 K). The echo-detected EPR spectra and transverse relaxation (phase memory) times T_2 were recorded using the standard two-pulse Hahn echo sequence $\pi/2$ – τ – π – τ –echo with pulse lengths 100/50 ns for π and $\pi/2$ pulses. Monoexponential analysis of echo decay vs. 2τ yields the corresponding T_2 value at certain magnetic field. CW EPR spectra were acquired using an X-band Bruker EMX spectrometer (9 GHz). In all experiments the sample was first shock-frozen in liquid nitrogen and then transferred into the cryostat. In this way we ensured that the sample was in glassy state at the beginning of each experiment. The heating/cooling rates were ca. 1 K/min; the sample was equilibrated for at least 10 minutes prior to each EPR measurement. All spectral simulations were done using EasySpin^{S5}.

Differential scanning calorimetry (DSC) measurements were performed using DSC 204 F1 (NETZSCH) equipment (see below).

II Differential scanning calorimetry (DSC) measurements

DSC measurements were performed using DSC 204 F1 (NETZSCH) equipment. Samples were placed in the closed and pressed alumina melting pot with 25 μ l volume. Setup calibration was done using indium (99,999%) and zinc (99.8+%) purchased from Sigma Aldrich. First, the samples were quickly (40° C/min) cooled to a temperature of -60° C, then the cooling went down to -120 C at a rate of 20° C/min, and, after holding at the lowest T , the sample was heated at a rate of 1° C/min to -60° C and then to the room temperature (25° C) at a speed of 10° C/min. Hexanol sample after exposure at the lowest T was heated at a rate of 1° C/min to the room temperature (25° C). Measured glass transition temperatures and the comparison with the literature data are listed in the Table S1. Figures S1-S3 show the original DSC data.

Table S1. Glass transition temperatures of studied samples determined by DSC.

Sample	$T_g^{[a]}$ / K	$T_g^{[b]}$ / K	$T_m^{[b]}$ / K
DMP	no data	194 ^{S6} , 193 ^{S4,S5} , 194.9 ^{S9}	278.7 ^{S8} , 274.4 ^{S9} , 275 ^{S10} , 273 ^{S11}
DEP	184.05	180.8 ^{S7} , 187 ^{S8} , 182.5 ^{S9} , 180 ^{S12}	240 ^{S8} , 233 ^{S11}
DBP	180.55	176 ^{S7} , 177 ^{S8} , 178.7 ^{S9} , 179 ^{S13} , 177.5 ^{S14}	238 ^{S5,S8,S10}
DOP	187.45	182.5 ^{S7} , 186 ^{S8} , 184.4 ^{S9} , 185.5 ^{S14}	223 ^{S8} , 248 ^{S11}
2-propanol	no data	115 ^{S15}	185 ^{S15}
Ethanol	no data	97.1 ^{S8} , 97 ^{S9,S10}	156 ^{S5,S10}
1-butanol	no data	111.7 ^{S8} , 113.6 ^{S9} , 118 ^{S16}	184.7 ^{S8} , 183.5 ^{S9} , 183 ^{S16}
1-pentanol	no data	121 ^{S8}	195 ^{S8}
1-hexanol	no data	129.9 ^{S8}	225.8 ^{S8}
Toluene	no data	117 ^{S5,S10} , 116 ^{S12}	180 ^{S5,S8} , 178 ^{S13} , 178.1 ^{S17}
Ethyl benzene	no data	115 ^{S5,S9}	178 ^{S8} , 178.1 ^{S17}
Butyl benzene	no data	128 ^{S5,S10}	185 ^{S5,S10}
[C ₁ MIm]BF ₄	no T_g^*	no data	376.55 ^{S18}
[C ₂ MIm]BF ₄	167.9*	186.15 ^{S19} , 180.15 ^{S20} , 184 ^{S21} , 183.75 ^{S22} , 181.15 ^{S23} , 178 ^{S24}	288.15 ^{S19,S20} , 288 ^{S21} , 287.15 ^{S22} , 286.15 ^{S23} , 284.15 ^{S24}
[C ₄ MIm]BF ₄	187.7*	188.15 ^{S23} , 202 ^{S18} , 176.15 ^{S25} , 188.85 ^{S26} , 185.85 ^{S27}	191 ^{S28} , 196.85 ^{S29}
[C ₅ MIm]BF ₄	181.3*	185.65 ^{S18} , 185.75 ^{S27}	no data
[C ₆ MIm]BF ₄	188*	190.75 ^{S18} , 187.55 ^{S27} , 194 ^{S30}	191.15 ^{S31}
[C ₈ MIm]BF ₄	188.8*	194.65 ^{S18} , 187.25 ^{S27} , 192 ^{S30}	194.15 ^{S31} , 193.15 ^{S32}

[a] This work, (*)^{S33}. [b] Literature data.

However, due to technical limitations of the equipment used, it was impossible to obtain reproducible results at the temperatures lower than 140 K.

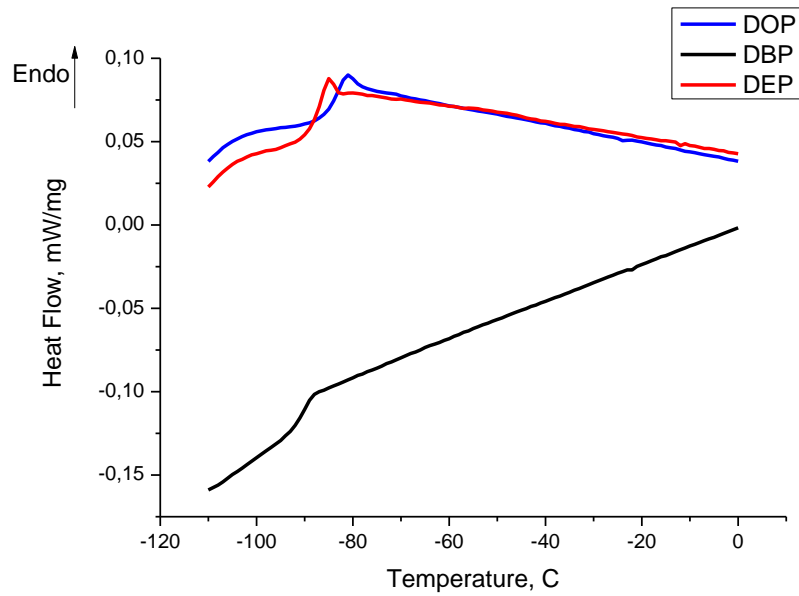


Figure S1. Overlay of DSC endotherms in the temperature range from -120 ° C to -20 ° C for DOP, DBP, DEP.

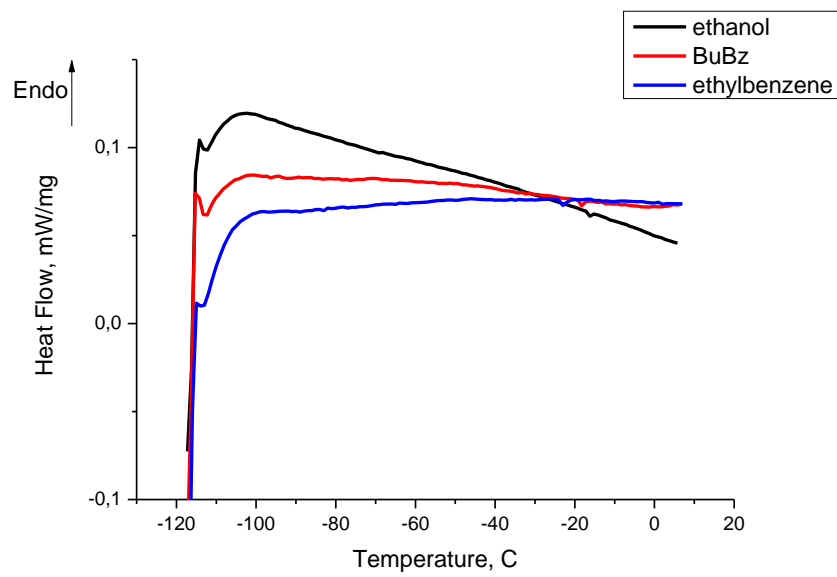


Figure S2. Overlay of DSC endotherms in the temperature range from -120 ° C to -20 ° C for ethanol, butylbenzene and ethylbenzene.

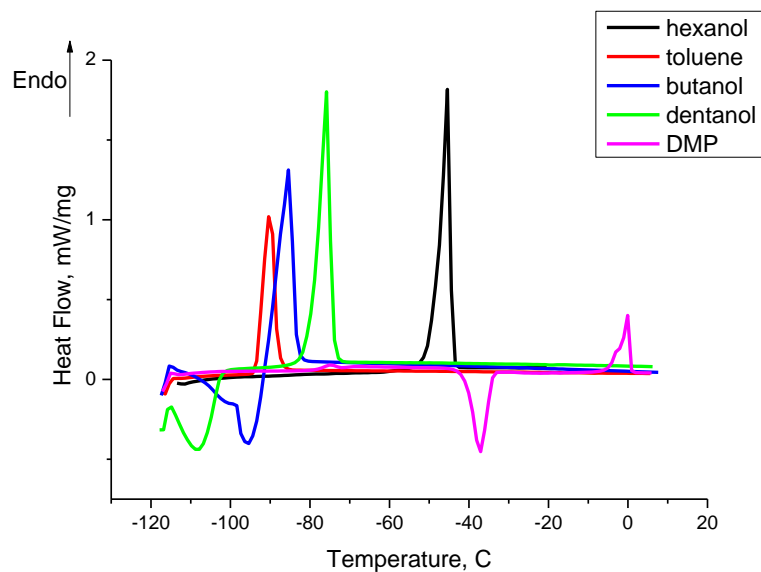


Figure S3. Overlay of DSC endotherms (differential) in the temperature range from -120° C to -20° C for hexanol, toluene, butanol, pentanol and DMP.

III Molecular dynamics: supplementary details

Molecular Dynamics (MD) simulations have been performed in GROMACS simulation package.^{S34} Initial force field parameters were obtained from LigParGen^{S35} and then partial charges were optimized based on B3LYP/def2-TZVP chelpg calculations.^{S36,S37} Force field parameters for TEMPO radical were adapted from Sezer et al.^{S38} MD simulations were performed in a cubic periodic box with a side length of 6 nm at room temperature. We have performed 400 ns NVT run at room temperature, prior the cell was relaxed and pressure equilibrated for 10 ns. We have used CSV thermostat^{S39} and Berendsen barostat.^{S40} Every 5 ns a snapshot was extracted from the room temperature trajectory. The temperature was then annealed separately to 160, 180, and 190 K in NPT ensemble over 1 ns, followed by a NVT run of 15 ns, where only last 10 ns were used for the data analysis. In total 81 snapshots were annealed, resulting in 1215 ns of data sampling for every low temperature.

We have used MDTraj^{S41} and VMD^{S42} for data analysis.

IV EPR of stochastic molecular librations

Stochastic librations or small-angle wobbles are limited stochastic orientation motions with small amplitudes that occur on a nanosecond time scale. These movements generated by thermal energy are inherent in organic glasses. When a spin probe (nitroxide commonly) is placed into the organic glass, the probe is exposed to the same librations imposed by surrounding glass. These librations cause magnetic interactions in spin probes and effectively induce an electron spin relaxation.

In general, pulse electron paramagnetic resonance is sensitive to the mobility of spin probes. In particular, the shape of the continuous wave (CW) EPR spectrum allows one to determine the rotational correlation time of a nitroxide radical. However, CW EPR is not sensitive in the case of small-angle wobbling ($<1^\circ$). Therefore, because of the impact of even small motions on electron spin relaxation rate, pulse EPR becomes an indispensable complementary technique.

Previously, in a series of works, Dzuba et.al.^{S43,S44} developed a powerful approach for studying stochastic librational motions in organic glasses and biopolymers using pulse EPR. This method employs nitroxide probes and is based on the measurements of transverse relaxation times (T_2) of nitroxide at two definite spectral positions.

The theoretical consideration of spin relaxation induced by the fast (sub-microsecond) stochastic molecular librations predicts the exponential decay of the two-pulse electron spin echo (ESE) signal in the Hahn sequence upon incrementing the time delay between two pulses. The decay rate is determined by spectral anisotropy at the position of the nitroxide spectrum (positions I and II in Fig.S4a). The spectrum of the nitroxide features three major components due to the hyperfine interaction (HFI) between the spin of unpaired electrons and the spin of nitrogen nucleus ($I=1$). The relaxation rate depends on the projection of the nuclear spin $\frac{1}{T_2}(m_I) \approx A + Bm_I + Cm_I^2$ ^{S45}, where A , B , C are functions dependent on correlation time, anisotropy of HFI and g-tensor. Hence, the central component (I) is influenced mainly by the anisotropy of the g-tensor, with the anisotropy of HFI being negligible; therefore, it possesses the smallest anisotropy and the narrowest linewidth. For the broadest high-field component (II), both anisotropies influence the spectral shape in an additive way, so it is the most anisotropic and the broadest one. Therefore, the decay rates for the field positions (I) and (II) are essentially different. However, there are other additive relaxation mechanisms contributing to the resulting T_2 values. Therefore, in order to elucidate pure libration-induced relaxation, it is necessary to subtract the relaxation rates (inverse relaxation times T_2) in the two spectral positions (I) and (II), as is illustrated in Fig. 4a.

As a result, we obtain pure libration-based contribution, which we denoted $L \equiv (1/T_2(II) - 1/T_2(I))$. Redfield relaxation theory shows that for fast (sub-

microsecond) and small-angle librations $L \approx C \langle \alpha^2 \rangle \tau_c$, where $\langle \alpha^2 \rangle$ is the mean square angular amplitude of motion, τ_c is the corresponding correlation time, and C is the numerical coefficient, whose value was semi-empirically determined to be $9 \cdot 10^{-16} \text{ s}^{-2}$ for nitroxide radicals.^{S44}

Measurement of the values of librational parameter at different temperatures yields a curve $L(T)$, whose shape is more informative than the absolute value of L at a certain temperature. Theory of atomic displacements predicts that $L(T)$ should linearly grow with temperature. Figure S4b sketches possible behaviors of $L(T)$ dependence. The onset of librations indicates the temperature where librations start to influence electron spin relaxation strong enough to be detected in ESE based T_2 measurements. The slope of the $L(T)$ curve characterizes the intensity of librations. When glass softens and transforms into a liquid, the amplitude of the nitroxide motions drastically grows, leading to a steep rise of $L(T)$ until T_2 becomes too short to be measured. Thus, in general, no other behaviors are to be expected for the $L(T)$, unless some structural rearrangements occur. There is no reason for $L(T)$ curve to change from a rising trend to a decrease as T increases, because kT driving librations does grow. Thus, any deviations from monotonic linear growth indicate some structural changes in the glassy matrix surrounding the nitroxide.

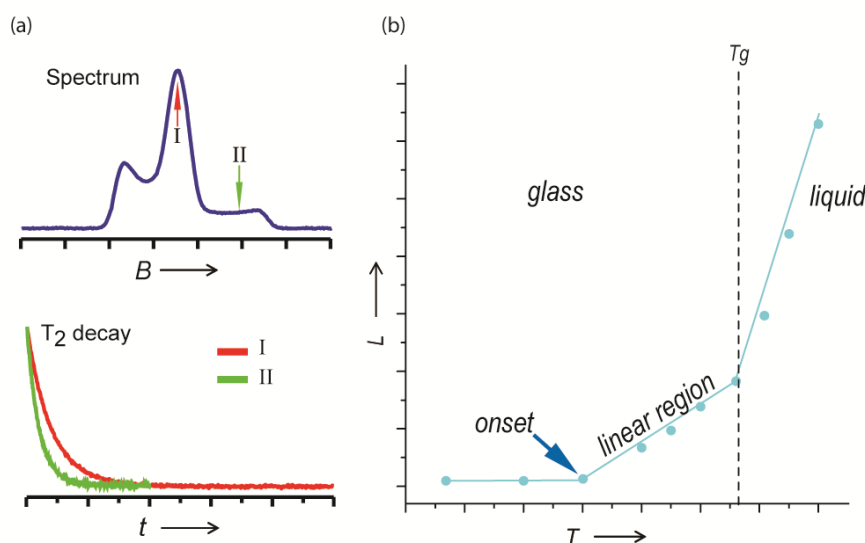


Figure S4. Sketch of the pulse EPR analysis scheme. (a) Two-pulse electron spin echo detected spectrum (top). The T_2 decay is measured by incrementing delay in $\pi/2 - \tau - \pi - \tau$ - echo sequence at two spectral positions I and II. Corresponding T_2 times are obtained by monoexponential analysis. (b) Typical $L(T)$ dependence showing low-temperature region of no librations, then their onset, linear region of effective librations, and, finally, transition into a liquid state with steep increase of molecular motion.

However in the previously studied ILs – as well as for other organic glasses with alkyl chains in this work - the $L(T)$ curve has three characteristic regions, that are marked as {a}, {b} and {c} in Figure S5. The rise of $L(T)$ function at ~ 70 K (region {a}) indicates the onset of stochastic molecular librations in IL. Further increase of the stochastic librations amplitude [growth of $L(T)$] is observed up to ~ 140 K (region {a})

in Fig.S5). However, then the anomalous suppression of the stochastic librations is found within $\sim 140\text{--}200$ K (region {b}), the exact range depends on the particular glass. At even higher temperatures $T > 200$ K, which are close to T_g of the studied ILs, the trend reverts to the rise again (region {c}), to be assigned to the unlocking of diffusive rotation of the radical in softened/melted glass. The linear growth of $L(T)$ in region {a} is a typical behavior that was observed previously in various organic glasses and biological membranes. The nonlinear region {b} of $L(T)$ is the most interesting and represents the structural rearrangements in alkyl-chain-containing glasses.

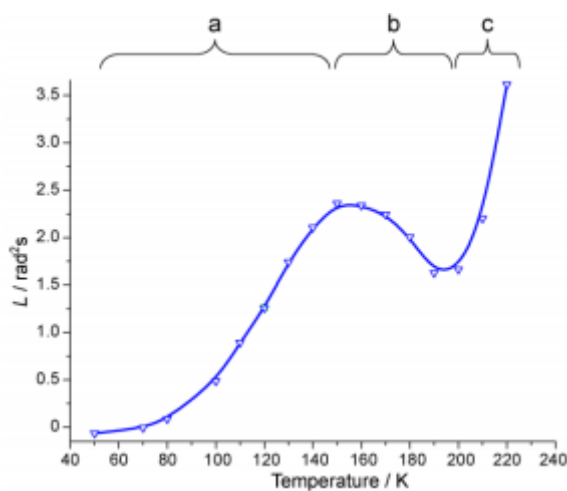


Figure S5. Representative schematic temperature dependence of the motional parameter L for nitroxide radical in ILs and some other organic glasses {a}, {b} and {c} indicate the motional regimes, see text for details. {b} is the region of anomaly.

V Temperature dependence of T_2 relaxation time

Figure S6 reports the data on the basis of which the $L(T)$ curves were calculated for each case. It shows the echo-detected EPR spectrum with two characteristic spectral positions I and II (Fig. S6a), individual T_2 measured at I and II positions for each sample, and their difference.

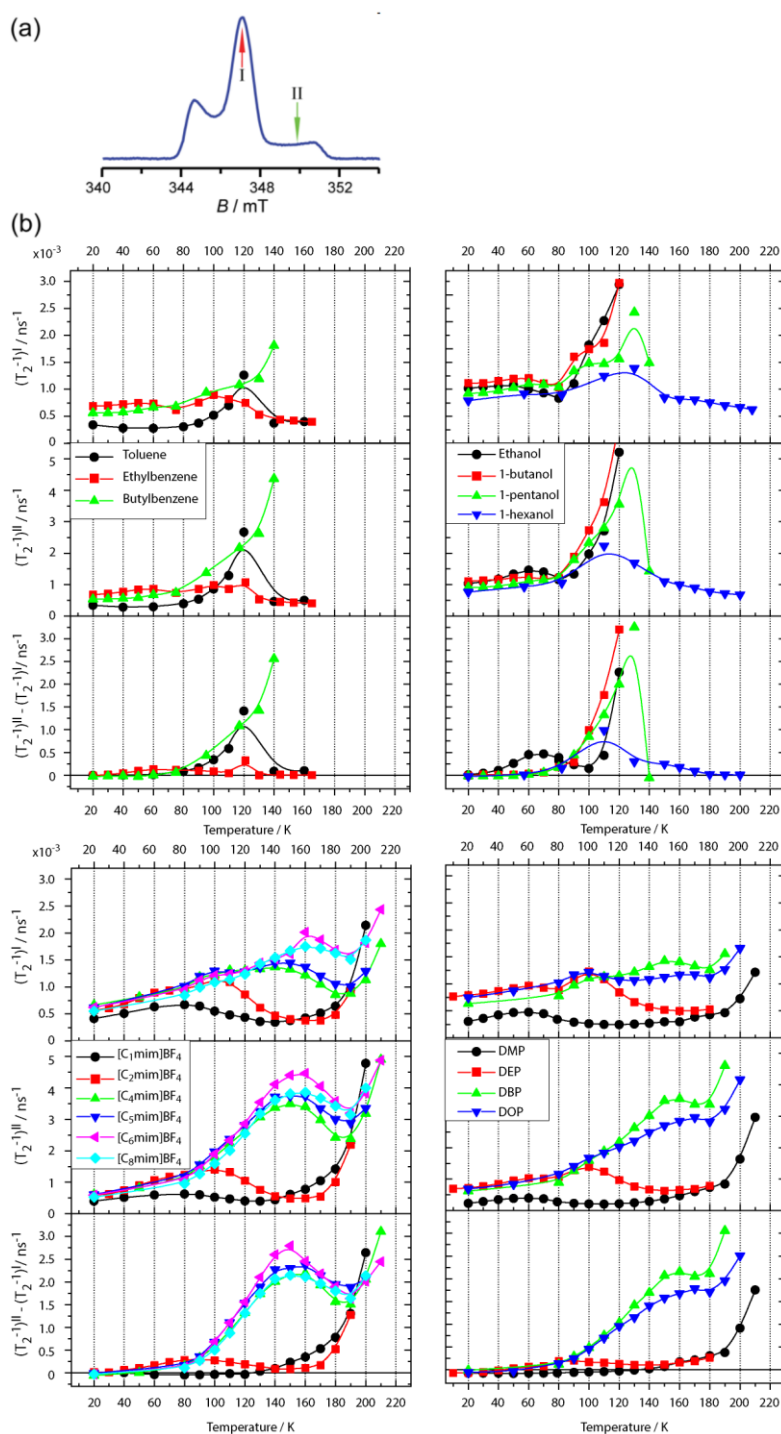


Figure S6. (a) Illustrative echo-detected spectrum with indicated field positions where T_2 was measured. (b) Temperature dependence of T_2^{-1} measured at low (I at Fig. S6a), high (II at Fig. S6a) field positions and their difference for all presented solvents. Lines represent the splines guiding the eye.

It is evident that the difference of inverse T_2 values (proportional to L) for $[\text{C}_1\text{mim}]\text{BF}_4$ is negative in the temperature range 20 – 130 K (Figure S6b), but in the final L value is biased to a zero level at low temperatures. The negative L depicts the domination of instantaneous diffusion processes when librations are negligible.^{S45} The shape of the echo detected spectrum (Figure S6a) indicates that the number of detected radical spins in field position (orientation) I is much higher compared to that in orientation II – as is reflected in their relative signal intensities. In other words, microwave pulses applied at field position I excite more electron spins compared to position II; therefore, flip-flop processes are more pronounced in position I and shorter T_2 relaxation time is obtained in this field position at low-temperature limit. As a result, L parameter gets the negative value.

It is well known that instantaneous diffusion process is generally temperature independent. At low temperatures radical libration mechanism is suppressed, and instantaneous diffusion process plays the dominant role and determines the obtained relaxation times. As the temperature is increased, the libration-induced relaxation takes over, and L becomes positive. Therefore, the negative L value at low temperatures (50 K and lower) can be considered as a constant background level.

VI Continuous wave EPR spectra

Figures S7-S9 show the CW EPR spectra of spin probe TEMPO-D₁₈ dissolved in the corresponding glass-formers. The computer simulations were performed using EasySpin.^{S5} Spectroscopic parameters used in simulations are listed in the Tables S2-S13.

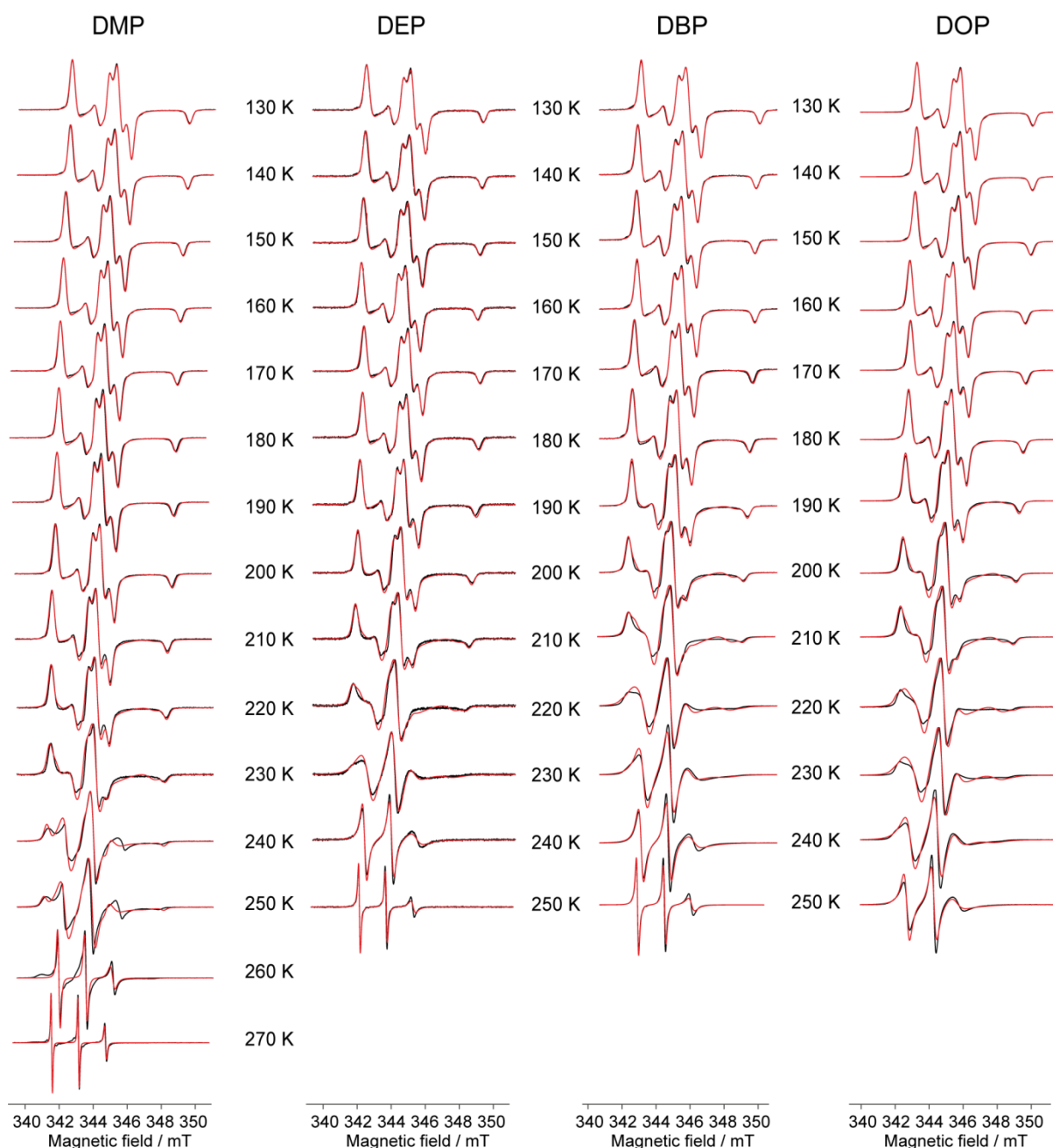


Figure S7. CW EPR spectra of TEMPO-D₁₈ dissolved in the corresponding phthalates vs. temperature. Black lines represent the experimental data, red ones - the simulation results.

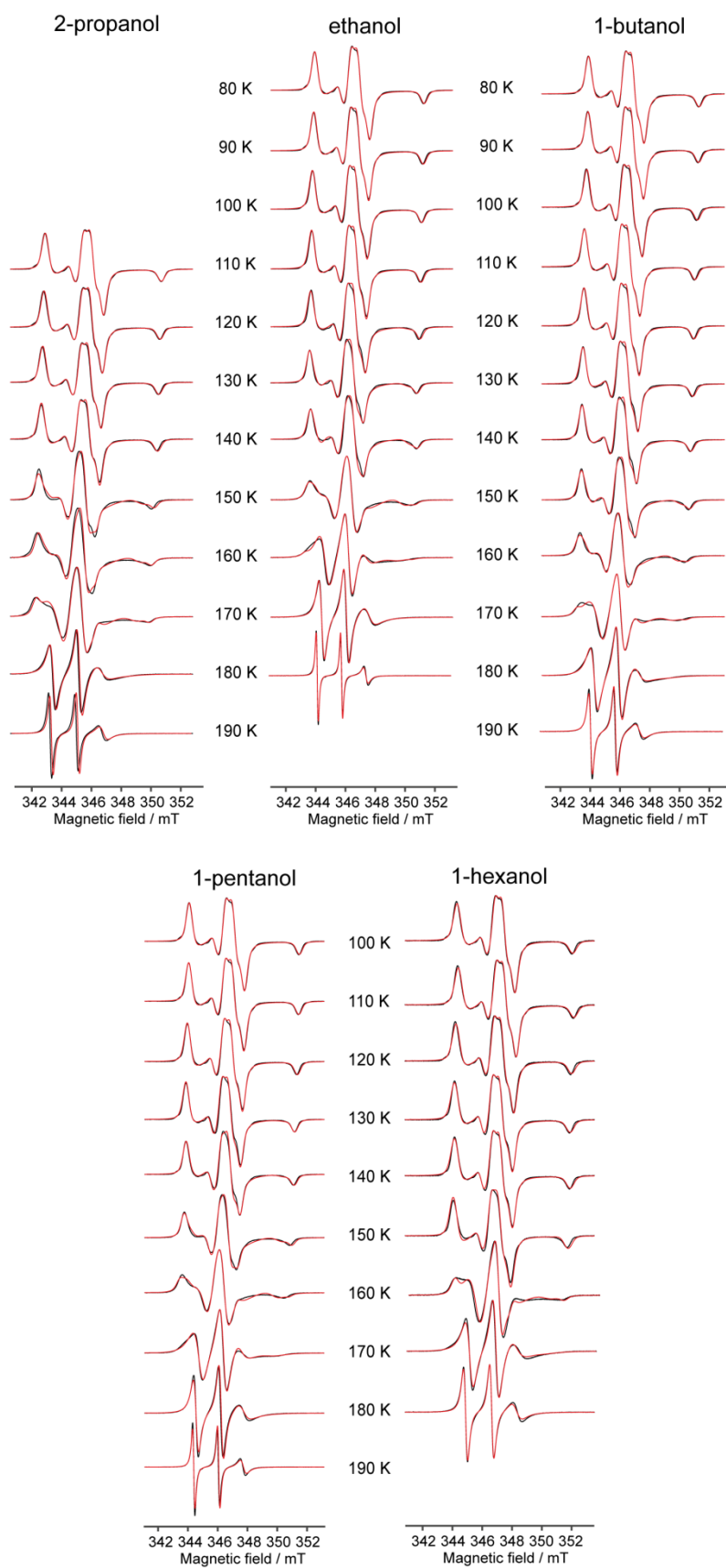


Figure S8. CW EPR spectra of TEMPO-D₁₈ dissolved in the corresponding alcohols vs. temperature. Black lines represent the experimental data, red ones - the simulation results.

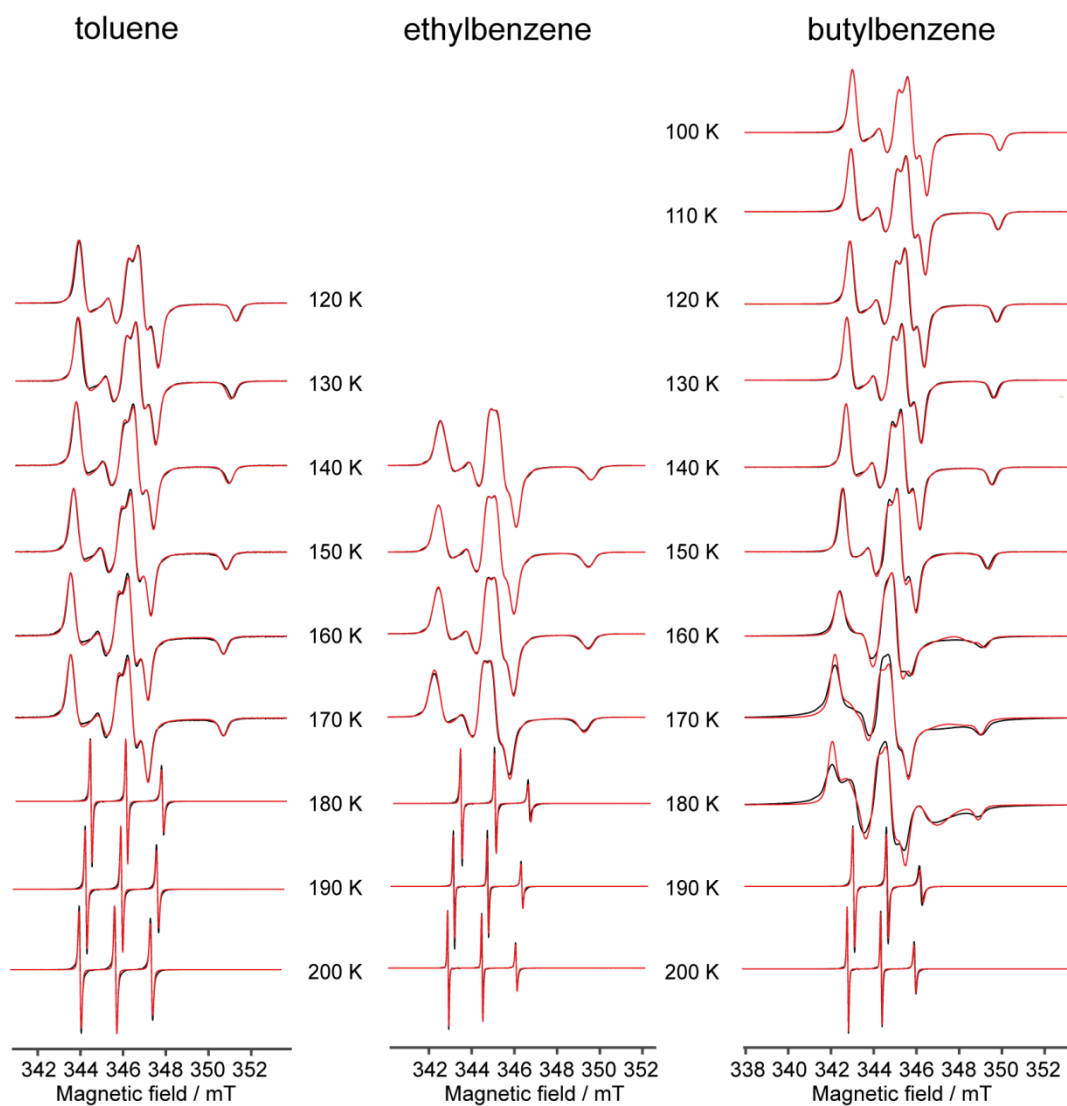


Figure S9. CW EPR spectra of TEMPO-D₁₈ dissolved in the corresponding alkyl benzenes vs. temperature. Black lines represent the experimental data, red ones - the simulation results.

Table S2. List of parameters used in simulation of CW EPR spectra of TEMPO-D₁₈ in DMP.

		Mobile fraction			Immobile fraction			
T / K	M	τ_c / ns	g-tensor	A-tensor / MHz	g-tensor	A-tensor / MHz	Astrain / MHz	
130	0	-	-		[2.0115 2.0079 2.0039]	[18.6 19.8 97.0]	[3.7 1.9 5.2]	
140	0	-						
150	0	-						
160	0	-						
170	0	-						
180	0	-						
190	0	-						
200	0.08	6.2	[2.0115 2.0079 2.0039]	[18.6 19.8 97.0]	-	-		
210	0.20	7.2		[18.6 19.8 95.8]			[18.6 19.8 95.8]	
220	0.33	8.5		[18.6 19.8 97.1]			[18.6 19.8 97.1]	
230	0.61	9.5					[18.6 19.8 99.6]	[18.6 19.8 99.6]
240	0.73	3.7					[18.6 19.8 96.2]	
250	0.84	3.4		[18.6 19.8 95.7]				
260	1	0.7						
270	1	0.3						

Table S3. List of parameters used in simulation of CW EPR spectra of TEMPO-D₁₈ in DEP.

		Mobile fraction			Immobile fraction			
T / K	M	τ_c / ns	g-tensor	A-tensor / MHz	g-tensor	A-tensor / MHz	Astrain / MHz	
130	0	-	-		[2.0112 2.0075 2.0036]	[19.0 19.9 96.6]	[4.6 1.4 5.5]	
140	0	-						
150	0	-						
160	0	-						
170	0	-						
180	0	-						
190	0.10	5.2						[2.0112 2.0075 2.0036]
200	0.25	8.0	[19.0 19.9 94.4]	[19.0 19.9 94.4]				
210	0.44	8.6	[19.0 19.9 102.1]					
220	0.75	8.5		[19.0 19.9 97.7]				
230	1	4.3		[19.0 19.9 96.4]				
240	1	2.2						
250	1	0.9						

Table S4. List of parameters used in simulation of CW EPR spectra of TEMPO-D₁₈ in DBP.

			Mobile fraction		Immobile fraction				
T / K	M	τ_c / ns	g-tensor	A-tensor / MHz	g-tensor	A-tensor / MHz	Astrain / MHz		
130	0	-	-		[2.0116 2.0075 2.0038]	[18.2 19.6 96.5]	[0 2.6 4.8]		
140	0	-							
150	0	-							
160	0	-							
170	0.08	4.3	[2.0116 2.0075 2.0038]	[18.2 19.6 95.7]	[18.2 19.6 95.7]	[18.2 19.6 94.1]	[18.2 19.6 99.9]		
180	0.16	7.5		[18.2 19.6 94.1]					
190	0.30	8.7		[18.2 19.6 99.9]					
200	0.52	9.1		[18.2 19.6 98.9]					
210	0.74	8.1		[18.2 19.6 101.2]					
220	0.98	5.1		[18.2 19.6 96.8]					
230	1	3.6		-					
240	1	2.2							
250	1	1.1							

Table S5. List of parameters used in simulation of CW EPR spectra of TEMPO-D₁₈ in DOP.

			Mobile fraction		Immobile fraction				
T / K	M	τ_c / ns	g-tensor	A-tensor / MHz	g-tensor	A-tensor / MHz	Astrain / MHz		
130	0	-	-		[2.0114 2.0076 2.0036]	[18.9 19.8 95.4]	[5.4 0 5.7]		
140	0	-							
150	0	-							
160	0.08	5.8	[2.0114 2.0076 2.0036]	[18.9 19.8 95.4]	[18.9 19.8 94.0]	[18.9 19.8 97.4]	[18.9 19.8 99.7]		
170	0.10	6.6		[18.9 19.8 94.0]					
180	0.12	8.1		[18.9 19.8 97.4]					
190	0.26	8.6		[18.9 19.8 99.7]					
200	0.50	9.3		[18.9 19.8 100.7]					
210	0.61	8.9		[18.9 19.8 98.6]					
220	0.91	6.8		-					
230	0.98	5.6							
240	1	3.9							
250	1	2.7							

Table S6. List of parameters used in simulation of CW EPR spectra of TEMPO-D₁₈ in 2-propanol.

		Mobile fraction			Immobile fraction		
T / K	M	τ_c / ns	g-tensor	A-tensor / MHz	g-tensor	A-tensor / MHz	Astrain / MHz
110	0	-	-		[2.01 2.0065 2.0026]	[18.8 19.0 101.5]	[3.1 9.9 6.9]
120	0	-					
130	0	-					
140	0.21	10.2	[2.01 2.0065 2.0026]	[18.8 19.0 101.5]	-	-	-
150	0.42	7.8		[18.8 19.0 99.5]			
160	0.56	6.4					
170	0.71	5.4					
180	1	2.6					
190	1	1.5					

Table S7. List of parameters used in simulation of CW EPR spectra of TEMPO-D₁₈ in ethanol.

		Mobile fraction			Immobile fraction		
T / K	M	τ_c / ns	g-tensor	A-tensor / MHz	g-tensor	A-tensor / MHz	Astrain / MHz
80	0	-	-		[2.0010 2.0065 2.0026]	[18.5 18.7 103.6]	[0 13.4 5.5]
90	0	-					
100	0	-					
110	0	-					
120	0.16	9.9	[2.0010 2.0065 2.0026]	[18.5 18.7 103.6]	-	-	-
130	0.32	11.6		[18.5 18.7 101.9]			
140	0.51	15.5					
150	0.82	7.9					
160	0.94	3.8					
170	1	2.0					
180	1	0.9	[18.5 18.7 102.6]				

Table S8. List of parameters used in simulation of CW EPR spectra of TEMPO-D₁₈ in 1-butanol.

		Mobile fraction			Immobile fraction		
T / K	M	τ_c / ns	g-tensor	A-tensor / MHz	g-tensor	A-tensor / MHz	Astrain / MHz
80	0	-	-		[2.0110 2.0075 2.0036]	[18.5 18.3 103.1]	[0 14.6 6.5]
90	0	-					
100	0	-					
110	0	-					
120	0	-					
130	0.07	7.5	[2.0110 2.0075 2.0036]	[18.5 18.3 102.6]	-	-	-
140	0.17	9.3		[18.5 18.3 101.6]			
150	0.44	12.7					
160	0.73	9.2					
170	0.88	4.8					
180	1	2.8					
190	1	1.6	[18.5 18.3 105.0]				

Table S9. List of parameters used in simulation of CW EPR spectra of TEMPO-D₁₈ in 1-pentanol.

			Mobile fraction		Immobile fraction		
T / K	M	τ_c / ns	g-tensor	A-tensor / MHz	g-tensor	A-tensor / MHz	Astrain / MHz
100	0	-	-		[2.0110 2.0076 2.0036]	[18.7 18.3 103.0]	[0 13.7 5.7]
110	0	-					
120	0	-					
130	0.09	8.6	[2.0110 2.0076 2.0036]	[18.7 18.3 101.8]	[18.7 18.3 101.8]		
140	0.24	8.3					
150	0.54	8.2					
160	0.83	7.0		[18.7 18.3 102.6]	[18.7 18.3 102.6]		
170	1	3.4		[18.7 18.3 108.2]	-		
180	1	2.1					
190	1	1.1	[18.7 18.3 104.8]				

Table S10. List of parameters used in simulation of CW EPR spectra of TEMPO-D₁₈ in 1-hexanol.

			Mobile fraction		Immobile fraction		
T / K	M	τ_c / ns	g-tensor	A-tensor / MHz	g-tensor	A-tensor / MHz	Astrain / MHz
100	0	-	-		[2.0102 2.0068 2.0028]	[18.5 17.9 102.3]	[0 14.9 8.6]
110	0	-					
120	0	-					
130	0	-					
140	0.24	4.4	[2.0102 2.0068 2.0028]	[18.5 17.9 102.3]	[18.5 17.9 98.0]		
150	0.42	7.4					
160	0.74	4.8		[18.5 17.9 98.0]			
170	1	2.7		[18.5 17.9 108.5]	-		
180	1	1.6		[18.5 17.9 105.3]			

Table S11. List of parameters used in simulation of CW EPR spectra of TEMPO-D₁₈ in toluene.

			Mobile fraction		Immobile fraction		
T / K	M	τ_c / ns	g-tensor	A-tensor / MHz	g-tensor	A-tensor / MHz	Astrain / MHz
120	0	-	-		[2.0096 2.0059 2.0019]	[18.0 19.7 94.2]	[4.0 2.0 6.8]
130	0	-					
140	0	-					
150	0	-				[18.0 19.7 94.3]	
160	0	-					
170	0	-				[18.0 19.7 93.7]	
180	1	0.2	[2.0096 2.0059 2.0019]	[18.0 19.7 93.8]	-		
190	1	0.1		[18.0 19.7 97.9]			
200	1	0.1		[18.0 19.7 95.6]			

Table S12. List of parameters used in simulation of CW EPR spectra of TEMPO-D₁₈ in ethylbenzene.

			Mobile fraction		Immobile fraction		
T / K	M	τ_c / ns	g-tensor	A-tensor / MHz	g-tensor	A-tensor / MHz	Astrain / MHz
150	0	-	-		[2.0102 2.0067 2.0028]	[19.4 20.3 98.0]	[7.3 9.9 10.6]
160	0	-					
170	0	-					
180	1	0.3	[2.0102 2.0067 2.0028]	[19.4 20.3 94.8]	-		
190	1	0.2					
200	1	0.1					

Table S13. List of parameters used in simulation of CW EPR spectra of TEMPO-D₁₈ in butylbenzene.

			Mobile fraction		Immobile fraction		
T / K	M	τ_c / ns	g-tensor	A-tensor / MHz	g-tensor	A-tensor / MHz	Astrain / MHz
100	0	-	-		[2.0116 2.0078 2.0037]	[18.6 19.4 96.4]	[2.0 5.3 5.8]
110	0	-					
120	0	-					
130	0	-					
140	0	-					
150	0.14	8.5	[2.0116 2.0078 2.0037]	[18.6 19.4 96.4]	-		
160	0.54	8.6					
170	0.35	5.5					
180	0.40	1.5					
190	1	0.4		[18.6 19.4 96.4]	-		
200	1	0.2		[18.6 19.4 94.6]			

References

- (S1) Read, R. R.; Foster, L. S.; Russell, A.; Simril, V. L. N-BUTYLBENZENE. *Org. Synth.* **1945**, 25 (September), 11. <https://doi.org/10.15227/orgsyn.025.0011>.
- (S2) Kirilyuk, I. A.; Polienko, Y. F.; Krumkacheva, O. A.; Strizhakov, R. K.; Gatilov, Y. V.; Grigor'ev, I. A.; Bagryanskaya, E. G. Synthesis of 2,5-Bis(Spirocyclohexane)-Substituted Nitroxides of Pyrroline and Pyrrolidine Series, Including Thiol-Specific Spin Label: An Analogue of MTSSL with Long Relaxation Time. *J. Org. Chem.* **2012**, 77 (18), 8016–8027. <https://doi.org/10.1021/jo301235j>.
- (S3) Rozantsev, E. G. *Free Nitroxyl Radicals.*; Ulrich H, Ed.; Plenum Press: New York, 1970.
- (S4) Shundrin, L. A.; Kirilyuk, I. A.; Grigor'Ev, I. A. 3-Carboxy-2,2,5,5-Tetra(2H3)Methyl-[4-2H(1H)]-3-Pyrroline-(1-15N)-1-Oxyl as a Spin Probe for in Vivo L-Band Electron Paramagnetic Resonance Imaging. *Mendeleev Commun.* **2014**, 24 (5), 298–300. <https://doi.org/10.1016/j.mencom.2014.09.017>.
- (S5) Stoll, S.; Schweiger, A. EasySpin, a Comprehensive Software Package for Spectral Simulation and Analysis in EPR. *J. Magn. Reson.* **2006**, 178 (1), 42–55. <https://doi.org/10.1016/j.jmr.2005.08.013>.
- (S6) Benazzouz, A.; Dudognon, E.; Correia, N. T.; Molinier, V.; Aubry, J. M.; Descamps, M. Interactions Underpinning the Plasticization of a Polymer Matrix: A Dynamic and Structural Analysis of DMP-Plasticized Cellulose Acetate. *Cellulose* **2017**, 24 (2), 487–503. <https://doi.org/10.1007/s10570-016-1148-y>.
- (S7) Nayak, S. K.; Murthy, S. S. N. Dielectric Relaxation Studies of Glass Formation in Some Esters of Phthalic Acid. *J. Chem. Phys.* **1993**, 99 (3), 1607–1613. <https://doi.org/10.1063/1.465329>.
- (S8) Saini, M. K.; Guo, Y.; Wu, T.; Ngai, K. L.; Wang, L.-M. Deviations of Dynamic Parameters Characterizing Enthalpic and Dielectric Relaxations in Glass Forming Alkyl Phosphates. *J. Chem. Phys.* **2018**, 149 (20), 204505. <https://doi.org/10.1063/1.5051570>.
- (S9) Murthy, S. S. N.; Gangasharan; Nayak, S. K. Novel Differential Scanning Calorimetric Studies of Supercooled Organic Liquids. *J. Chem. Soc. Faraday Trans.* **1993**, 89 (3), 509. <https://doi.org/10.1039/ft9938900509>.
- (S10) Ebert, G. W.; Juda, W. L.; Kosakowski, R. H.; Ma, B.; Dong, L.; Cummings, K. E.; Phelps, M. V. B.; Mostafa, A. E.; Luo, J. Carboxylation and Esterification of Functionalized Arylcopper Reagents. *J. Org. Chem.* **2005**, 70 (11), 4314–4317. <https://doi.org/10.1021/jo047731s>.
- (S11) Kinjo, N.; Nakagawa, T. Viscoelastic Behavior of Some Di(Normal Alkyl) Phthalates. *Bull. Chem. Soc. Jpn.* **1978**, 51 (4), 1024–1026. <https://doi.org/10.1246/bcsj.51.1024>.

- (S12) Capaccioli, S.; Ruocco, G.; Zamponi, F. Dynamically Correlated Regions and Configurational Entropy in Supercooled Liquids. *J. Phys. Chem. B* **2008**, *112* (34), 10652–10658. <https://doi.org/10.1021/jp802097u>.
- (S13) Surovtsev, N. V. On the Glass-Forming Ability and Short-Range Bond Ordering of Liquids. *Chem. Phys. Lett.* **2009**, *477* (1–3), 57–59. <https://doi.org/10.1016/j.cplett.2009.05.078>.
- (S14) Ngai, K. L.; Kamińska, E.; Sekuła, M.; Paluch, M. Primary and Secondary Relaxations in Bis-5-Hydroxypentylphthalate Revisited. *J. Chem. Phys.* **2005**, *123* (20). <https://doi.org/10.1063/1.2121667>.
- (S15) Talón, C.; Ramos, M. A.; Vieira, S.; Shmyt'ko, I.; Afonikova, N.; Criado, A.; Madariaga, G.; Bermejo, F. J. Thermodynamic and Structural Properties of the Two Isomers of Solid Propanol. *J. Non. Cryst. Solids* **2001**, *287* (1–3), 226–230. [https://doi.org/10.1016/S0022-3093\(01\)00565-8](https://doi.org/10.1016/S0022-3093(01)00565-8).
- (S16) Kurita, R.; Tanaka, H. On the Abundance and General Nature of the Liquid-Liquid Phase Transition in Molecular Systems. *J. Phys. Condens. Matter* **2005**, *17* (27). <https://doi.org/10.1088/0953-8984/17/27/L01>.
- (S17) Sorek, A.; Atzmon, N.; Dahan, O.; Gerstl, Z.; Kushisin, L.; Laor, Y.; Mingelgrin, U.; Nasser, A.; Ronen, D.; Tsechansky, L.; Weisbrod, N.; Graber, E. R. “Phytoscreening”: The Use of Trees for Discovering Subsurface Contamination by VOCs. *Environ. Sci. Technol.* **2008**, *42* (2), 536–542. <https://doi.org/10.1021/es072014b>.
- (S18) Holbrey, J. D.; Seddon, K. R. Tetrafluoroborates ; Ionic Liquids and Ionic Liquid Crystals. **1999**, 2133–2139.
- (S19) Sato, T.; Masuda, G.; Takagi, K. Electrochemical Properties of Novel Ionic Liquids for Electric Double Layer Capacitor Applications. *Electrochim. Acta* **2004**, *49* (21), 3603–3611. <https://doi.org/10.1016/j.electacta.2004.03.030>.
- (S20) Zhou, Z. Bin; Matsumoto, H.; Tatsumi, K. Structure and Properties of New Ionic Liquids Based on Alkyl- and Alkenyltrifluoroborates. *ChemPhysChem* **2005**, *6* (7), 1324–1332. <https://doi.org/10.1002/cphc.200500094>.
- (S21) Noda, A.; Hayamizu, K.; Watanabe, M. Pulsed-Gradient Spin-Echo ¹H and ¹⁹F NMR Ionic Diffusion Coefficient, Viscosity, and Ionic Conductivity of Non-Chloroaluminate Room-Temperature Ionic Liquids. *J. Phys. Chem. B* **2001**, *105* (20), 4603–4610. <https://doi.org/10.1021/jp004132q>.
- (S22) Earle, M. J.; McCormac, P. B.; Seddon, K. R. Regioselective Alkylation in Ionic Liquids. *Chem. Commun.* **1998**, No. 20, 2245–2246. <https://doi.org/10.1039/a806328a>.
- (S23) Nishida, T.; Tashiro, Y.; Yamamoto, M. Physical and Electrochemical Properties of 1-Alkyl-3-Methylimidazolium Tetrafluoroborate for Electrolyte. *J. Fluor. Chem.* **2003**, *120* (2), 135–141. [https://doi.org/10.1016/S0022-1139\(02\)00322-6](https://doi.org/10.1016/S0022-1139(02)00322-6).
- (S24) McEwen, A. B. Electrochemical Properties of Imidazolium Salt Electrolytes for

- Electrochemical Capacitor Applications. *J. Electrochem. Soc.* **1999**, *146* (5), 1687. <https://doi.org/10.1149/1.1391827>.
- (S25) Huddleston, J. G.; Visser, A. E.; Reichert, W. M.; Willauer, H. D.; Broker, G. A.; Rogers, R. D. Characterization and Comparison of Hydrophilic and Hydrophobic Room Temperature Ionic Liquids Incorporating the Imidazolium Cation. *Green Chem.* **2001**, *3* (4), 156–164. <https://doi.org/10.1039/b103275p>.
- (S26) Xu, W.; Wang, L. M.; Nieman, R. A.; Angell, C. A. Ionic Liquids of Chelated Orthoborates as Model Ionic Glassformers. *J. Phys. Chem. B* **2003**, *107* (42), 11749–11756. <https://doi.org/10.1021/jp034548e>.
- (S27) Strehmel, V.; Laschewsky, A.; Krudelt, H.; Wetzal, H.; Görnitz, E. Free Radical Polymerization of Methacrylates in Ionic Liquids. In *Ionic Liquids in Polymer Solvents*; CS, B., RD, R., Eds.; American Chemical Society, Washington DC, 2005; pp 17–36. <https://doi.org/10.1021/bk-2005-0913.ch002>.
- (S28) Suarez, P. A. Z.; Selbach, V. M.; Dullius, J. E. L.; Einloft, S.; Piatnicki, C. M. S.; Azambuja, D. S.; De Souza, R. F.; Dupont, J. Enlarged Electrochemical Window in Dialkyl-Imidazolium Cation Based Room-Temperature Air and Water-Stable Molten Salts. *Electrochim. Acta* **1997**, *42* (16), 2533–2535. [https://doi.org/10.1016/S0013-4686\(96\)00444-6](https://doi.org/10.1016/S0013-4686(96)00444-6).
- (S29) Park, H. S.; Choi, Y. S.; Jung, Y. M.; Hong, W. H. Intermolecular Interaction-Induced Hierarchical Transformation in 1D Nanohybrids: Analysis of Conformational Changes by 2D Correlation Spectroscopy. *J. Am. Chem. Soc.* **2008**, *130* (3), 845–852. <https://doi.org/10.1021/ja073074k>.
- (S30) Crosthwaite, J. M.; Muldoon, M. J.; Dixon, J. K.; Anderson, J. L.; Brennecke, J. F. Phase Transition and Decomposition Temperatures, Heat Capacities and Viscosities of Pyridinium Ionic Liquids. *J. Chem. Thermodyn.* **2005**, *37* (6), 559–568. <https://doi.org/10.1016/j.jct.2005.03.013>.
- (S31) Berthod, A.; Ruiz-Ángel, M. J.; Carda-Broch, S. Ionic Liquids in Separation Techniques. *J. Chromatogr. A* **2008**, *1184* (1–2), 6–18. <https://doi.org/10.1016/j.chroma.2007.11.109>.
- (S32) Law, G.; Watson, P. R. Surface Tension Measurements of N-Alkylimidazolium Ionic Liquids. *Langmuir* **2001**, *17* (20), 6138–6141. <https://doi.org/10.1021/la010629v>.
- (S33) Bakulina, O. D.; Ivanov, M. Y.; Prikhod'ko, S. A.; Pylaeva, S.; Zaytseva, I. V.; Surovtsev, N. V.; Adonin, N. Y.; Fedin, M. V. Nanocage Formation and Structural Anomalies in Imidazolium Ionic Liquid Glasses Governed by Alkyl Chains of Cations. *Nanoscale* **2020**, *12* (38), 19982–19991. <https://doi.org/10.1039/d0nr06065h>.
- (S34) Lindahl; Abraham; Hess; Spoel, van der. GROMACS 2020 Source Code. **2020**. <https://doi.org/10.5281/ZENODO.3562495>.
- (S35) Dodda, L. S.; De Vaca, I. C.; Tirado-Rives, J.; Jorgensen, W. L. LigParGen Web Server: An Automatic OPLS-AA Parameter Generator for Organic Ligands. *Nucleic Acids Res.* **2017**, *45* (W1), W331–W336.

<https://doi.org/10.1093/nar/gkx312>.

- (S36) Lu, T.; Chen, F. Multiwfn: A Multifunctional Wavefunction Analyzer. *J. Comput. Chem.* **2012**, *33* (5), 580–592. <https://doi.org/10.1002/jcc.22885>.
- (S37) Neese, F.; Wennmohs, F.; Becker, U.; Riplinger, C. The ORCA Quantum Chemistry Program Package. *J. Chem. Phys.* **2020**, *152* (22). <https://doi.org/10.1063/5.0004608>.
- (S38) Sezer, D.; Freed, J. H.; Roux, B. Parametrization, Molecular Dynamics Simulation, and Calculation of Electron Spin Resonance Spectra of a Nitroxide Spin Label on a Polyalanine α -Helix. *J. Phys. Chem. B* **2008**, *112* (18), 5755–5767. <https://doi.org/10.1021/jp711375x>.
- (S39) Bussi, G.; Donadio, D.; Parrinello, M. Canonical Sampling through Velocity Rescaling. *J. Chem. Phys.* **2007**, *126* (1). <https://doi.org/10.1063/1.2408420>.
- (S40) Hess, B.; Bekker, H.; Berendsen, H. J. C.; Fraaije, J. G. E. M. LINCS: A Linear Constraint Solver for Molecular Simulations. *J. Comput. Chem.* **1997**, *18* (12), 1463–1472. [https://doi.org/10.1002/\(SICI\)1096-987X\(199709\)18:12<1463::AID-JCC4>3.0.CO;2-H](https://doi.org/10.1002/(SICI)1096-987X(199709)18:12<1463::AID-JCC4>3.0.CO;2-H).
- (S41) McGibbon, R. T.; Beauchamp, K. A.; Harrigan, M. P.; Klein, C.; Swails, J. M.; Hernández, C. X.; Schwantes, C. R.; Wang, L. P.; Lane, T. J.; Pande, V. S. MDTraj: A Modern Open Library for the Analysis of Molecular Dynamics Trajectories. *Biophys. J.* **2015**, *109* (8), 1528–1532. <https://doi.org/10.1016/j.bpj.2015.08.015>.
- (S42) Humphrey, W.; Dalke, A.; Schulten, K. VMD: Visual Molecular Dynamics. *J. Mol. Graph.* **1996**, *14* (1), 33–38. [https://doi.org/10.1016/0263-7855\(96\)00018-5](https://doi.org/10.1016/0263-7855(96)00018-5).
- (S43) Dzuba, S. A. Libration Motion of Guest Spin Probe Molecules in Organic Glasses: CW EPR and Electron Spin Echo Study. *Spectrochim. Acta - Part A Mol. Biomol. Spectrosc.* **2000**, *56* (2), 227–234. [https://doi.org/10.1016/S1386-1425\(99\)00234-6](https://doi.org/10.1016/S1386-1425(99)00234-6).
- (S44) Isaev, N. P.; Dzuba, S. A. Fast Stochastic Librations and Slow Rotations of Spin Labeled Stearic Acids in a Model Phospholipid Bilayer at Cryogenic Temperatures. *J. Phys. Chem. B* **2008**, *112* (42), 13285–13291. <https://doi.org/10.1021/jp805794c>.
- (S45) Eaton, S. S.; Eaton, G. R. Relaxation Mechanisms. In *eMagRes*; John Wiley & Sons, Ltd: Chichester, UK, 2016; Vol. 5, pp 1543–1556. <https://doi.org/10.1002/9780470034590.emrstm1507>.